Functional Implications of the Propionate 7−Arginine 220 Interaction in the FixLH Oxygen Sensor from *Bradyrhizobium japonicum*†

V. Balland,‡ L. Bouzhir-Sima,§ E. Anxolabéhère-Mallart,⊥ A. Boussac,‡ M. H. Vos,§ U. Liebl,§ and T. A. Mattioli*,‡

Laboratoire de Biophysique du Stress Oxydant, SBE/DBJC and CNRS URA 2096, CEA/Saclay, 91191 Gif-sur-Yvette Cedex, France, Laboratoire d'Optique et Biosciences, INSERM U696, CNRS UMR 7645, Ecole Polytechnique-ENSTA, 91128 Palaiseau, France, and Laboratoire de Chimie Inorganique, UMR CNRS 8613, 91405 Orsay Cedex, France

Received August 25, 2005; Revised Manuscript Received December 19, 2005

ABSTRACT: *Bj*FixL from *Bradyrhizobium japonicum* is a heme-based oxygen sensor implicated in the signaling cascade that enables the bacterium to adapt to fluctuating oxygen levels. Signal transduction is initiated by the binding of O_2 to the heme domain of *Bj*FixL, resulting in protein conformational changes that are transmitted to a histidine kinase domain. We report structural changes of the heme and its binding pocket in the Fe^{II} deoxy and Fe^{III} met states of the wild-type *Bj*FixLH oxygen sensor domain and four mutants of the highly conserved residue arginine 220. UV−visible, electron paramagnetic resonance, and resonance Raman spectroscopies all showed that the heme iron of the R220H mutant is unexpectedly six-coordinated at physiological pH in the Fe^{III} state but undergoes pH- and redox-dependent coordination changes. This behavior is unprecedented for FixL proteins, but is reminiscent of another oxygen sensor from *E. coli*, *Ec*Dos. All mutants in their deoxy states are five-coordinated Fe^{II}, although we report rupture of the residue 220−propionate 7 interaction and structural modifications of the heme conformation as well as propionate geometry and flexibility. In this work, we conclude that part of the structural reorganization usually attributed to O_2 binding in the wild-type protein is in fact due to rupture of the Arg220−P7 interaction. Moreover, we correlate the structural modifications of the deoxy Fe^{II} states with k_{on} values and conclude that the Arg220−P7 interaction is responsible for the lower O_2 and CO k_{on} values reported for the wild-type protein.

Heme-based sensors are key regulators of adaptive responses to environmental fluctuations and control the activity of a neighboring domain (*1*, *2*). One class of sensor proteins contains the heme cofactor within a sensory PAS domain. PAS domains exhibit a conserved structural fold and are proposed to share a common conformational flexibility, potentially related to a mechanism for signal transduction (*3*).

The rhizobial FixL proteins are the best studied heme-PAS sensors and respond to fluctuating oxygen levels in the bacterial environment. FixL proteins possess a histidine kinase domain, responsible for the phosphorylation of a transcription factor FixJ, and a heme domain (FixLH[1]), where O_2 binding and initial oxygen sensing occur (*4*). The FixL sensor domains contain a *b*-type heme as a prosthetic group with a proximal histidine as axial ligand, and signal transduction is driven by structural modifications of the heme pocket upon ligand binding. More recently, other heme-PAS sensors were identified, such as NPAS2, sensing CO (*5*), *Ax*PDEA1, sensing O_2 (*6*), and *Ec*Dos, which seems to be sensitive to the O_2 level (*7*) and the redox state of the iron (*8*, *9*). The crystallographic data reported for the Fe^{II} and Fe^{III} states of *Ec*Dos indicate ligand switching upon oxidation, consistent with previous spectroscopic studies. Upon oxidation, two water molecules enter the heme pocket and replace the Met95 ligand, leading to a six-coordinated low-spin aquo−Fe^{III} complex (*8*).

Crystallographic structures of the deoxy (Fe^{2+}) and met (Fe^{3+}) redox states of FixL hemodomains indicate a highly hydrophobic heme pocket associated with a five-coordinated high-spin iron (*10*−*14*). The high degree of hydrophobicity of the heme pocket is due to the presence of a hydrophobic triad corresponding to residues Ile215/Leu236/Ile238 in *Bj*FixLH (*10*) (Figure 1) and Ile209/Leu230/Val232 in *Rm*FixL (*13*), whose side chains point toward the heme iron. Unlike myoglobin (*15*), no water molecule is reported in the

† T.A.M. gratefully acknowledges financial support from the Regional Council of the Ile-de-France for an equipment grant (S. E. S. A. M. E.).

* To whom correspondence should be addressed: Service de Bioénergétique, Département de Biologie Joliot-Curie, CEA Saclay, 91191, Gif-sur-Yvette Cedex, France. Phone: +33 169 08 41 66. Fax: +33 169 08 87 17. E-mail: tony.mattioli@cea.fr.

‡ Laboratoire de Biophysique du Stress Oxydant.

§ Laboratoire d'Optique et Biosciences.

⊥ Laboratoire de Chimie Inorganique.

[1] Abbreviations: *Ax*PDEA1, phosphodiesterase 1 from *Acetobacter xylinum*; *Bj*, *Bradyrhizobium japonicum*; 5c, five-coordinated; 6c, six-coordinated; *Ec*Dos, direct oxygen sensor from *E. coli*; EPR, electron paramagnetic resonance; FixL*, soluble truncated FixL; FixLH, hemodomain of FixL; FG loop, Thr209 to His220 in *Bj*FixLH; Hb, Hemoglobin; HI, hydrophobicity index; HS, high spin; LS, low spin; Mb, myoglobin; NHE, normal hydrogen electrode; NPAS2, neuronal PAS domain protein 2; P-6 and P-7, heme propionate 6 and 7, respectively; *Rm*, *Rhizobium meliloti*; RR, resonance Raman; *SW*, sperm whale; WT, wild type.

10.1021/bi051696h CCC: $33.50
Published on Web 01/31/2006

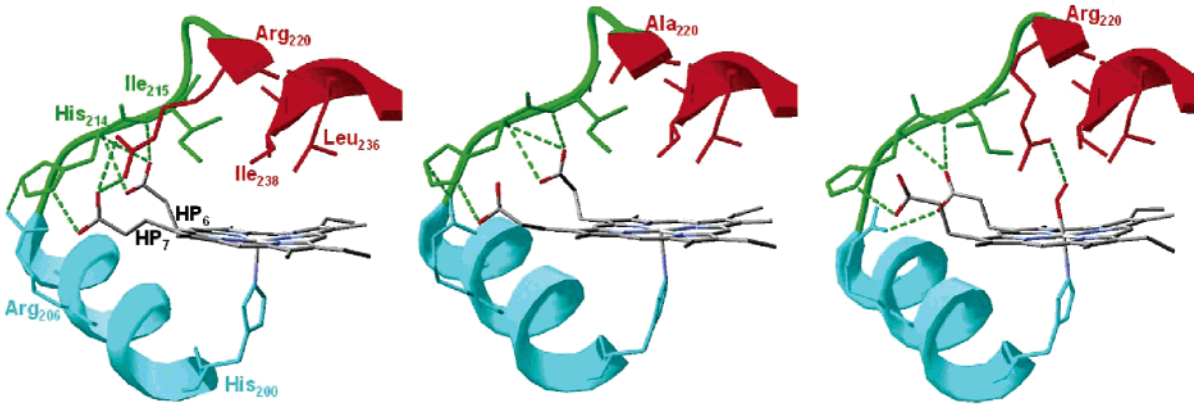

FIGURE 1: Crystallographic structures of the met wild-type (left, PDB entry 1DRM (*10*)), R220A met (middle, DB entry 1Y28 (*17*)), and oxy wild-type (right, PDB entry 1DP6 (*11*)) states of *Bj*FixLH. Arg220 (or Ala220), Leu236, Ile238, and G β-sheets are in red, Arg206 and F α-helix are in cyan, His214, Ile215, and FG loops are represented in green. The heme propionates 6 and 7 are labeled HP6 and HP7, respectively.

vicinity of the heme iron. Ile209 has been shown to be predominantly responsible for the high degree of hydrophobicity of the *Rm*FixL heme pocket and to prevent entrance of a water molecule into the distal pocket (*16*). In both the Fe^{II} and the Fe^{III} states of the wild-type FixL proteins, the conserved hydrophilic positively charged Arg220 (*Bj*FixL) or Arg214 (*Rm*FixL) is interacting with the solvent-exposed heme propionate 7 group and water molecules and is thus pointing away from the iron atom (*10*, *11*, *13*). *Bj*FixL Arg220 is proposed to be a key residue for signal transduction; however, this residue is not essential to maintain the heme pocket structure in the met state. Indeed, the X-ray structure of the Fe^{III} R220A mutant of *Bj*FixLH has been reported (*17*), in which no shift of the FG loop or of the Ile215/Leu236/Ile238 residues is observable as compared to the wild-type protein (Figure 1). This mutant exhibits fully active histidine kinase activity in both its Fe^{II} and Fe^{III} states.

O_2 is a potent inhibitor of FixL phosphorylation activity (*17*, *18*). Upon O_2 binding, structural changes in the FG loop ("FG loop switch") occur as deduced from X-ray crystallography (*11*). This stuctural change is somehow associated with enzymatic inhibition, presumably via structural changes at the kinase domain, through a mechanism not yet understood.

Upon diatomic ligand binding (O_2, CO, NO, or CN^-) to *Bj*FixLH, the heme becomes six-coordinated (6c) low-spin (LS) and the crystallographic structures exhibit one common feature, that is, the movement of the Ile238 side chain toward the heme vinyl substituents to decrease the steric constraints around the binding site (*11*, *12*). On the basis of a recent high-resolution structure of the Fe^{II}−CO state, it is also proposed that the Ile215 and Leu236 side chains are slightly displaced upon ligand fixation (*14*). These observations further support the early proposal of Perutz et al. (*19*) that conformational changes responsible for kinase inactivation are partially driven by steric hindrance between the heme ligand and the hydrophobic triad residues. Still, CO and NO are only weak inhibitors of the histidine kinase domain (*17*, *18*). In the particular case of strong histidine kinase inhibitors such as O_2, modifications of the heme pocket structure are noted (*11*, *12*), including a shift of the critical FG loop, together with a large displacement of Ile215 and Arg220, the latter being shifted toward the heme pocket where it interacts via hydrogen bonds with both the bound ligand and a surrounding water molecule (Figure 1) (*12*). This results in highly efficient O_2 geminate recombination (*20*) together with strong inhibition of the histidine kinase domain (*17*). Thus, positions of residues Ile215 and Arg220 are indicative for structural modifications of the FG loop and the heme pocket resulting in signal transduction and efficient histidine kinase inactivation. Recently, we demonstrated that both the movement of Arg220 inside the heme pocket and its influence on the π-acidity properties of O_2 play a crucial role in the structural reorganization of the heme pocket implied in signal transduction (*21*). These observations are consistent with the recent hypothesis of multicoordinate ligand-coupled signaling (*22*).

In the present article, we describe the structural modifications of *Bj*FixLH in the Fe^{II} deoxy and Fe^{III} met resting states resulting from mutation of Arg220. The point mutations were chosen to modify the electrostatic properties and H-bonding capabilities of the residue 220, with minor steric modifications of the side chain (e.g., Arg220 was substituted by His, Ile, Gln, and Glu). A resonance Raman characterization of the Fe^{II}−O_2 and Fe^{II}−CO states of the same series of mutants as well as the measured association and dissociation rates for O_2 and CO binding was recently reported by us (*21*). In the present article, resonance Raman spectroscopy, EPR, and spectroelectrochemical titrations were used to obtain further detailed insight in the structural and electrostatic role of Arg220 in both the deoxy Fe^{II} and met Fe^{III} redox states, linked to the association rate for O_2 and CO binding. Particuliar attention was accorded to the R220H mutant, which exhibits strong pH-dependent modification of its heme pocket structure in the met Fe^{III} state as compared to the wild-type protein. Together with previous results obtained for O_2 fixation, our data indicate that this mutant is oxygen- as well as redox-sensitive, properties that are proposed to play important roles in *Ec*Dos, another O_2 sensor (*7*−*9*).

EXPERIMENTAL PROCEDURES

Protein Expression and Purification. Wild-type and mutant protein overexpression in *E. coli* and purification were performed as previously described in Balland et al. (*21*).

Sample Preparation. All protein samples were prepared in 50 mM Tris buffer at pH 7.4 and in 50 mM acetate buffer at pH 4.40. The deoxy form of *Bj*FixLH was prepared by

reduction in deoxygenated buffer by addition of freshly prepared degassed sodium dithionite (200 μM final concentration) (Sigma) stock solution in 18 MΩ deionized water. These samples were conditioned under argon gas, anaerobically sealed with gastight rubber septums, and transferred, when required, using gastight syringes (Hamilton).

UV−Visible Absorption Spectroscopy. Optical absorbance measurements were made using a UVIKON 922 (Kontron) spectrophotometer with a 70-μL airtight quartz cell (Hellma) with a path length of 1 cm. The protein concentration was 20 μM, and the measurements were performed at ambient temperature. For the pH dependence analysis of the R220H mutant, 5 μL of a concentrated protein solution in 50 mM Tris-HCl (pH 7.4) was diluted into 100 μL of a 100 mM buffer solution at the required pH. Acetate buffer was used for pH in the range [3.8−5.0]. MES buffer was used for pH in the range [5.2−6.7]. Phosphate buffer was used for pH in the range [6.0−8.0]. Tris-HCl buffer was used for pH in the range [7.0−8.0]. At pH 3.8, we noticed in time an increase in the baseline of the UV−visible absorption spectra of the proteins, probably due to some denaturation of the protein. For the electrochemical, EPR, and RR spectroscopic measurements reported here, samples were never poised below pH 4.4, where we observed no indications of protein denaturation.

EPR Measurements. X-band EPR spectra were recorded using a standard ER 4102 (Bruker) X-band resonator with a Bruker ESP300 X-band spectrometer equipped with an Oxford Instruments cryostat (ESR 900). The samples were frozen at 198 K and degassed as previously described (*23*) and then transferred to a liquid nitrogen bath (77 K) before measurements were taken at 4 and 26 K. Determination of *g*-values was done using an ER032M gaussmeter (Bruker). Protein samples were 100 μL of a 100 μM solution. Concentrated protein solutions were obtained by using a 10 kDa cutoff Centricon membrane concentrator (Amicon). At pH 7.4, Tris-HCl buffer was not used because of its sensitive temperature dependence (*24*), and it was replaced by a 100 mM Hepes buffer at pH 7.45.

Spectroelectrochemical Titrations. The UV−visible optical absorption spectra during oxidation−reduction titrations were recorded using a Varian 5E spectrophotometer. The thin layer cell used for room-temperature UV−vis experiments was previously described (*25*). The optical path length of the cell was 0.5 mm. A gold mesh working electrode was immersed in the optical cell. A platinum wire and SCE electrodes were used as counter and reference electrodes, respectively. The potential was controlled by a potentiostat (EGG PAR M362), and the current at the counter electrode was measured. The following redox mediators (2 μM each) were added to the sample solution: phenazine methosulfate, gallocyanine, indigo trisulfonate, 2-hydroxy-1,4-naphthoquinone, anthraquinone 2-sulfonate, benzyl viologen, and methyl viologen. The FixLH solution (25 μM) containing the mediator dyes was degassed and flushed with argon prior to the measurements, and 100 μL of the solution was transferred into the optical cell. The upper reservoir section (7 mL) of the electrochemical cell was filled with a degassed buffer solution containing the mediator dyes at the same concentration. All potential values are given using NHE as reference.

During the electrochemical redox titrations, the electronic absorption spectra were measured after the current reached a value < 0.5 μA (10−15 min). The potential was varied from 250 to −150 mV vs NHE. The absorption spectrum at 250 mV was identical to that of ferric FixLH as isolated, exhibiting a Soret band maximum at 395 nm. A −150 mV potential was applied for 20 min before oxidative titration from −150 mV to 250 V. After the oxidative titration, the potential was swept negatively to re-reduced the protein. The data were analyzed using the Nernst equation (*26*): Fraction $Fe^{II} = \{\exp[(E_{1/2} - E_m)*nF/RT] + 1\}^{-1}$, where n is the number of electrons, E_m is the measured potential, and $E_{1/2}$ is the midpoint potential of interest ($F = 96493$ J·V^{-1}, $R = 8.31$ J·mol^{-1}·K^{-1}).

Resonance Raman Spectroscopy. Resonance Raman spectra were recorded as described previously (*24*) using a modified single-stage spectrometer T64000 (Jobin-Yvon) equipped with a liquid nitrogen-cooled back-thinned CCD detector and 1800 grooves/mm holographic gratings. Samples for the resonance Raman measurements were prepared at a protein concentration of 20 μM. Spectra were recorded at room temperature in a spinning cell (diameter 2 mm) to prevent photodissociation and avoid local thermal degradation of the protein during the measurements. In some cases, RR spectra were recorded at low temperature (15 K) using a circulating cold He gas cryostat (Janis Research, STVP-100) to compare with low temperature EPR measurements. To accurately determine small differences in RR band frequencies, the monochromator was calibrated using the laser excitation wavelength and a saturated sulfate solution and samples were recorded the same day without changing light excitation/collection geometry. Spectral frequencies are estimated to have reproducibilities of ±1 cm^{-1}. Reported spectra at 413.1 nm were the result of the averaging of, typically, 200 single spectra, each recorded with 30 s of CCD exposure time. Reported spectra at 441.6 nm were the result of the averaging of approximately 600 single spectra recorded with 5 s of exposure time. Spectral resolution was about 3 cm^{-1}. Baseline corrections were performed using GRAMS 32 software (Galactic Industries). The band assignments are proposed by analogy with myoglobin (*27*).

RESULTS

UV−Visible Spectroscopy. The UV−visible absorption spectra of the *Bj*FixLH wild-type and mutant proteins were recorded in the range 200−800 nm at pH 7.4; representative spectra are shown in Figure 2. For the Fe^{II} states (Table 2), the mutations did not significantly alter the observed Soret bands around 431 nm (Table 2), characteristic of five-coordinated high-spin (5c HS) heme b-type Fe^{II} states (*28*). For the Fe^{III} states (Table 1), the iron is 5c HS with a Soret band at 395 nm for the wild-type protein (Figure 2) as for the R220Q, R220I, and R220E mutants. However, for the R220H mutant in the Fe^{III} state at pH 7.4 (Figure 2), the Soret band maximum is shifted to 408 nm at the same pH conditions as WT and the other mutants; there are also spectral differences observed in the 500−550 nm region. These spectral differences are attributed to a six-coordination state for the high-spin Fe^{III} in the met R220H mutant. The observed Soret band maximum for the R220H mutant (408 nm) occurs at a wavelength similar to that of the 6c HS Fe^{III} states of *SW*Mb and of the I209H *Rm*FixL mutant (Table 1), which both have a water molecule coordinated to the Fe^{III}

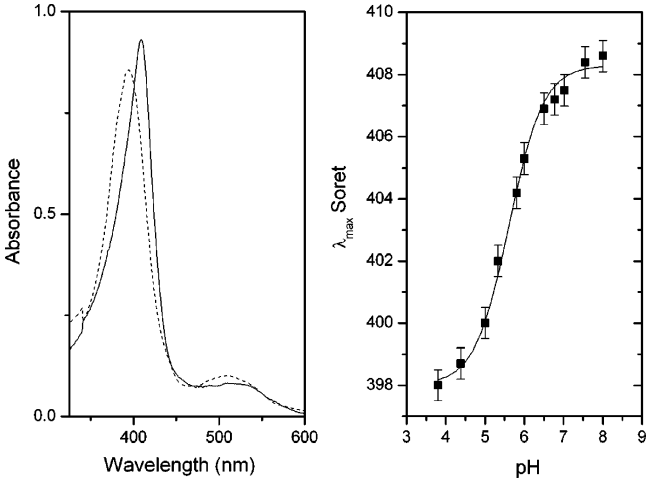

FIGURE 2: (Left) UV−visible spectra recorded at pH 7.4 for wild-type *Bj*FixLH (—) and the R220H mutant (− − −). (Right) pH titration of the R220H mutant obtained by UV−visible absorption. The solid line corresponds to the two-state Henderson−Hasselbach fit.

in the distal pocket (*29*, *30*). The pH dependence of the UV−visible spectrum from the R220H mutant was studied in the pH range 3.8−8.0. Upon acidification of the solution, the Soret band maximum progressively blue-shifted, down to 397 nm at pH 3.8. Thus, at pH 3.8 the R220H spectrum appears as that of WT protein pH 7.4 indicative of 5c HS Fe^{III}. This pH-dependent behavior implies that the sixth ligand on the R220H heme Fe^{III} center at pH 7.4 is displaced in acidic media. We analyzed the spectrophotometric titration curve using a simple two-state Henderson−Hasselbach plot (Figure 2) and found that a single protonatable group is involved with an apparent value of $pK_a = 5.7$.

EPR Measurements. The Fe^{III} met states of the *Bj*FixLH wild-type protein and mutants were studied by EPR spectroscopy to confirm the spin states of the iron. For the WT protein, the EPR spectrum indicates an $S = {}^5/_2$ high-spin Fe^{III} state with resonances at $g_1 = 6.16$, $g_2 = 5.51$, but g_3 is not clearly defined (Figure 3, Table 1). The percent rhombicity R for the wild-type *Bj*FixLH is 4.0 ($R = [\Delta g/16] \times 100$, where $\Delta g = |g_1 - g_2|$ (*31*)). These g and R values are similar to those reported for 5c HS Fe^{III} states for *Rm*FixL with $R = 2.5$ (*30*) and for the H64L mutant of *SW*Mb with $R = 3.4$ (Table 1) (*29*). For the R220I and Q mutants, the g values are very similar to those of the wild-type protein (Table 1), indicating that the Fe^{III} coordination geometry and immediate environment are not modified upon mutation.

For the R220H mutant, the EPR spectrum recorded at pH 7.45 exhibits a $g = 6$ signal with three components (Figure 3): a sharp $g = 5.88$ signal and two other resonances around $g = 6.30$ and $g = 5.30$. These features are very similar to those reported for the HS Fe^{III} state of the *SW*Mb H64Q mutant in Hepes buffer (Table 1) (*29*) where it had first been proposed that the three resonances were due to two species in solution, one being five-coordinated and a second being six-coordinated with a water ligand. However, a later high-resolution crystal structure of the H64Q mutant indicates a bound water molecule (*15*). Thus, for the *Bj*FixLH R220H mutant it is most likely that the EPR spectrum is reflecting two six-coordinated HS conformers of the protein, one axial corresponding to the $g = 5.88$ resonance and a second more rhombic with $R = 6.2$. This conclusion is fully consistent with the RR data obtained at 15 K and at room temperature which indicate the presence of only 6c HS heme Fe^{III} species (see below).

For the *Bj*FixLH R220H mutant here, the EPR spectrum is modified upon acidification of the solution. At pH 4.4, the spectrum exhibits two components corresponding to the following g values, $g_1 = 6.06$ and $g_2 = 5.54$ (g_3 is not detected) and $R = 3.25$, which are similar to those of the wild-type Fe^{III} *Bj*FixLH, implying a 5c HS Fe^{III} and thus the removal of the sixth Fe^{III} ligand in the R220H mutant upon acidification.

Electrochemical Redox Titrations. Figure 4B shows the oxidative redox titrations at pH 7.4 of the Fe^{II} deoxy *Bj*FixLH WT and the R220I, R220Q, and R220E mutants. Full oxidation−reduction reversibility without hystereses and well-defined isobestic points at 415 and 458 nm were observed in the UV−visible absorption spectra (Figure 4). The measured heme iron $E_{1/2}$ midpoint potential value for the wild-type *Bj*FixLH was 68 mV vs NHE. For the R220Q, R220I, and R220E mutants, $E_{1/2}$ values were found at 41, 38, and 24 mV, respectively (Table 1). Thus, replacement of the nearby positively charged arginine residue by the electrically neutral isoleucine or glutamine residues both lowered the $E_{1/2}$ potential of the heme iron by about 30 mV. The trend and magnitude of this effect is completely consistent with the removal of a positive charge in the vicinity of the heme group (*32*). For the R220E mutant, the $E_{1/2}$ potential value is found at 24 mV, about 50 mV lower than WT, and about 20 mV more negative than that seen for the mutants with electrically neutral amino acid residues at position 220. We argue that the additional lowering of the midpoint potential for the R220E mutant reflects a deprotonated negatively charged glutamate residue near the heme. This proposal is further supported by analysis of the Raman spectrum of the R220E mutant (see below).

The electrochemical titration of the R220H mutant is fully reversible at pH 7.4 with well-defined isobestic points at 419 and 462 nm. The measured heme iron $E_{1/2}$ midpoint potential value for this mutant is 40 mV vs NHE (see Supporting Information Figure S1), a value very similar to that reported for *SW* myoglobin (Table 1) that exhibits a six-coordinated Fe^{III} state and a five-coordinated Fe^{II} state (*33*). The reversibility of the redox titration is indicative of a rapid chemical equilibrium between the 5c and 6c redox states, and the 40 mV redox potential reported corresponds to the redox couple His−Fe^{III}−X/His−Fe^{II}, where X is the sixth ligand in the oxidized state. Therefore, this redox potential may not be directly compared to those reported for the wild-type protein and the other mutants as it does not implicate the same redox couple.

Resonance Raman Spectroscopy. Fe^{III} Met FixLH States. In the high-frequency region (Figure 5), the coordination/spin state-sensitive ν_2 and ν_3 and redox state ν_4 marker bands of the WT *Bj*FixLH met protein at pH 7.4 are observed at 1564, 1494, and 1373 cm^{-1}, respectively, clearly indicating a ferric 5c HS heme iron (*34*, *35*). The RR spectra are similar for the R220I, Q, and E mutants and indicate that the spin and coordination states of the iron do not change upon Arg220 replacement by these residues, consistent with the UV−visible absorption spectra (Table 1). However, the core-size-sensitive ν_3 and ν_2 modes downshift by 2 or 3 cm^{-1} in these mutants, indicating an expanded heme core size (*34*),

Table 1: Spectroscopic Properties of the Fe^{III} Met States for WT *Bj*FixLH and Mutants at Position 220

	ligation	λ_{Soret}	$E_{1/2}$	*g* values	ν_4	ν_3	ν_2	ref
*Bj*FixL	His/	395	−	−	1370	1493	1562	35
*Bj*FixLH WT	His/	395	68	6.16, 5.51	1373	1494	1564	this work
R220H pH 7.4	His/OH_2	408	40	6.30, 5.88, 5.30	1370	1478	1556	this work
R220H pH 4.4	His/	398	−	6.06, 5.54	1371	1492	1562	this work
R220Q	His/	395	39	6.20, 5.45	1370	1492	1561	this work
R220I	His/	395	42	6.20, 5.45	1370	1494	1563	this work
R220E	His/	396	24	−	1371	1493	1562	this work
*SW*Mb WT	His/OH_2	409	59	5.97[b]	1373	1485	1567	29, 33
H64Q	His/OH_2	409	−	6.29, 5.95, 5.53[b]	−	−	−	29
H64L	His/	395	84	6.09, 5.54, 2.0[b]	−	−	−	29, 33
*Rm*FixL WT	His/	397	−	6.16, 5.75	1371	1492	1562	30
I209H	His/OH_2	409	−	−	1370	1478	1554	16
I210H	His/His	414	−	−	1374	1505	1562	16
*Ec*DOS WT	His/OH_2	416	67	−	1372	1505	1577	7, 8, 35, 50

[a] λ values are given in nanometers. Potentials are given in mV versus NHE. Raman vibrational frequencies are given in cm^{-1}. [b] EPR values are taken from the measurements in the Hepes buffer at pH 7.

Table 2: Spectroscopic Properties of the Fe^{II} Deoxy States for WT *Bj*FixLH and Mutants at Position 220[a]

	λ_{Soret}	ν_{Fe-His}	ν_8	$I_{\nu 8}$[b]	P-6[c]	I_{P-6}[b]	P-7[d]	I_{P-7}[b]	ν_4	ν_3	ν_2	ref
*Bj*FixLH						−						
WT		218		−	nr[e]		nr	−	1353	1469	1555	35
WT	431	219	341	1.4	365 1His214 1Ile215	0.6	381 1Arg220 1His214	0.5	1354	1469	1555	this work
R220H	434	219	344	1.1	362	0.6	376	0.9	1352	1468	1554	this work
R220Q	432	217	341	1.2	363	0.6	378	0.7	1351	1467	1553	this work
R220I	432	216	344	0.8	363	0.5	376	0.9	1351	1467	1553	this work
R220E	432	217	341	1.4	362	0.6	376 (sh)	0.4	1352	1466	1553	this work
*SW*Mb												
WT	433	218	342	−	370[f] 1Arg45	−	370[f] 1Ser92 1His97	−	1357	1472	1564	27

[a] λ values are given in nanometers. Potentials are given in mV versus NHE. Raman vibrational frequencies are given in cm^{-1}. k_{on} values are given in 10^{-4} M^{-1} s^{-1}. [b] The band intensity is given relative to the ν_7 band at 675 cm^{-1} used to normalize the spectra. [c] $\delta_{C\beta CcCd}$ bending mode for the propionate 6 group. Residues listed are those donating H-bond to the carboxylate group according to the respective X-ray crystal structure. The number preceding the residue indicates the number of H-bonds donated by that residue. [d] $\delta_{C\beta CcCd}$ bending mode for the propionate 7 group. Same as footnote b. [e] nr − not reported. [f] Denotes the observation of only one band for the two propionate groups.

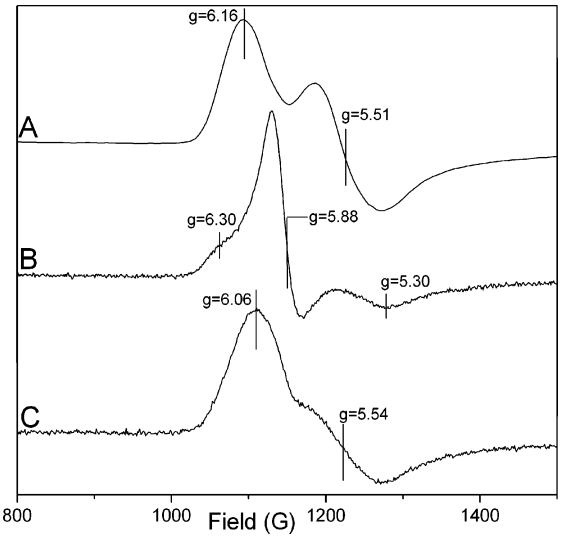

FIGURE 3: EPR spectra recorded for *Bj*FixLH WT pH 7.45 (A), R220H pH 7.45 (B), and R220H pH 4.4 (C). Sample concentration: 50 μM, temperature 15 K. Samples were prepared in a 100 mM Hepes buffer for pH 7.45, and a 100 mM acetate buffer for pH 4.4.

corresponding to flattening of the heme macrocycle, as was observed in the crystal structure of the *Bj*FixLH R220A in its Fe^{III} met state (*17*).

In stark contrast, the RR spectrum of the R220H mutant recorded at pH 7.4 shows major differences compared to those of WT and the other mutants (Figure 5). The ν_4 oxidation marker band is downshifted to 1370 cm^{-1} but still clearly indicates an Fe^{III} redox state. The ν_2 and ν_3 spin state and coordination marker bands have also significantly downshifted from 1564 to 1556 cm^{-1} and from 1494 to 1478 cm^{-1}, respectively. These values clearly indicate that in the R220H mutant at pH 7.4, the Fe^{III} center is six-coordinated HS (*36*), which is further supported by the ν_{38} mode ($C_\beta-C_\beta$ stretch) frequency at 1509 cm^{-1}, downshifted by 15 cm^{-1} as compared to WT protein (1524 cm^{-1}). These frequencies are characteristic of a 6c HS Fe^{III} ion and similar to those of *Rm*FixL I209H mutant (ν_3 = 1478 cm^{-1}, ν_{38} = 1510 cm^{-1}, ν_2 = 1554 cm^{-1}) (*16*) and most myoglobins (Table 1) (*37*), where a water molecule, exerting a weak ligand field, is coordinated to the heme iron. These RR conclusions of a 6c HS Fe^{III} state for the R220H mutant are consistent with the UV−visible and EPR results reported in Table 1. Because the EPR spectra were recorded at liquid helium temperatures, we also recorded the RR spectrum of the R220H as a function of temperature down to 15 K; the RR data still indicated that the 6c HS ferric state did not change (data not shown). Upon acidification of the R220H solution, the RR spectrum changes, and at pH 4.4, it is similar to that of

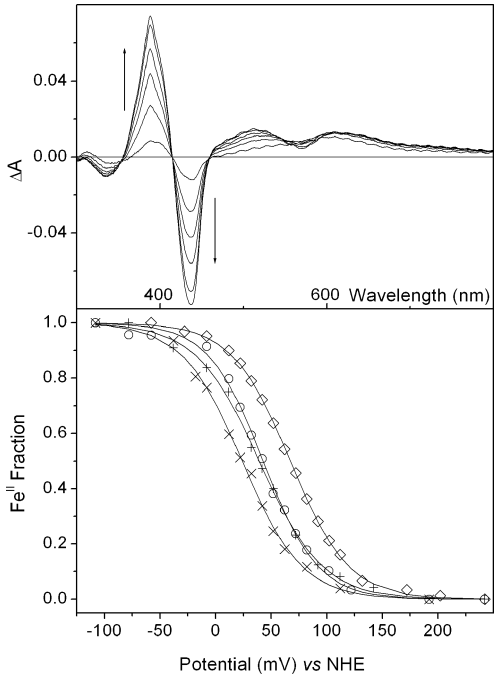

FIGURE 4: (Top) UV−visible spectral changes recorded during oxidative titration at pH 7.4 for WT *Bj*FixLH compared to that of the Fe^{II} deoxy species. (Bottom) Oxidative titration at pH 7.4 for WT (◇), R220Q (○), R220I (+), and R220E (×). Solid lines are the fitted Nernst curves. When the data sets were fit allowing $E_{1/2}$ and n to vary, values of $n = 0.90-1.03$ were obtained.

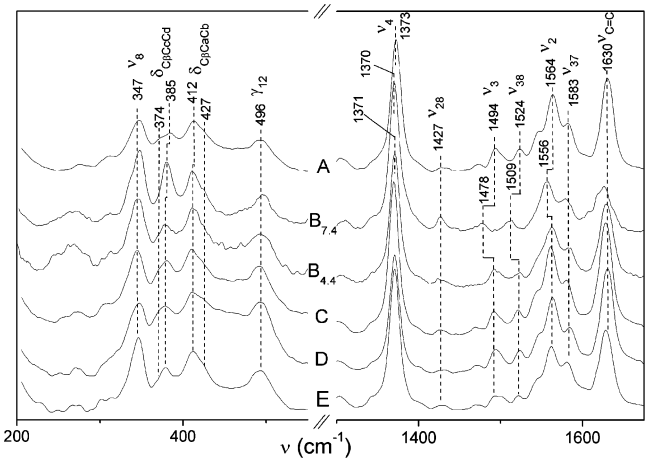

FIGURE 5: RR spectra of the met-FixL forms recorded with $\lambda = 413.1$ nm. (A) WT FixLH pH 7.4; ($B_{7.6}$) R220H pH 7.4; ($B_{4.4}$) R220H pH 4.4; (C) R220Q pH 7.4; (D) R220I pH 7.6; (E) R220E pH 7.4.

the other R220 mutants at pH 7.4, with ν_2 and ν_3 frequencies characteristic of a five-coordinated high-spin Fe^{III} state (Figure 5; Table 1).

The modes of the propionate and vinyl substituents are sensitive probes for the orientation and position of the porphyrin in the heme pocket and their interactions with the surrounding residues (*38*, *39*). The vinyl stretching mode $\nu_{C=C}$ is observed as one intense RR band at 1630 cm^{-1} for WT Fe^{III} *Bj*FixLH, and in the low-frequency region one intense band at 412 cm^{-1} and a shoulder around 427 cm^{-1} are attributed to the vinyl bending modes $\delta_{C\beta CcCd}$ (Figure 5) (*27*). Both the $\nu_{C=C}$ and $\delta_{C\beta CcCd}$ frequencies are conserved upon mutation of Arg220 to Ile, Gln, and Glu, indicating that the position of the heme in the heme pocket is not affected by

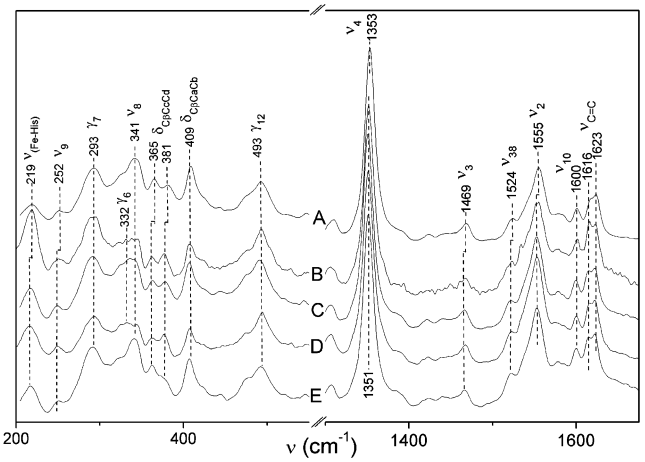

FIGURE 6: RR spectra of the deoxy-FixL forms recorded with $\lambda = 441.6$ nm at pH 7.4. (A) WT FixLH; (B) R220H; (C) R220Q; (D) R220I; (E) R220E. High-frequency spectra were normalized versus ν_4 band intensity. low-frequency spectra were normalized versus the ν_7 band intensity (at 675 cm^{-1}).

the mutation. In the low-frequency area, two propionate bending modes $\delta_{C\beta CcCd}$ are observed at 385 and 374 cm^{-1} for the WT *Bj*FixLH protein. Such a splitting of the propionate bending modes has been reported for some met hemoglobins (*37*). According to the met-*Bj*FixLH X-ray structure, propionate 7 is hydrogen-bonded to both Arg220 and His214, whereas propionate 6 is hydrogen-bonded to protein backbone carbonyl (Figure 1) (*11*). On the basis of the X-ray crystallographic structure of wild-type FixLH and the R220A mutant (*11*, *17*), we may assign these two bands to each propionate group based on their expected H-bonding patterns deduced from the structures. Upon mutation of Arg220, one propionate bending mode at 385 cm^{-1} is observed to downshift by 5 cm^{-1}, indicating weakening of the H-bond to the propionate group (*41*). This observation is fully consistent with the removal of Arg220 since two H-bonds between the propionate 7 group and the Arg220 are proposed in the WT met-*Bj*FixLH structure (*11*). Thus, for the WT Fe^{III} met-*Bj*FixLH protein, the 385 cm^{-1} $\delta_{C\beta CcCd}$ mode can be attributed to propionate 7 and the 374 cm^{-1} band to the propionate 6 group.

Fe^{II} Deoxy FixLH States. Porphyrin Modes. The ν_3 (1467−1469 cm^{-1}) and the ν_4 (1351−1353 cm^{-1}) frequencies in the resonance Raman spectrum of WT deoxy-*Bj*FixLH and all four mutant proteins (Figure 6) clearly indicate the heme iron for wild type and the mutants to be all in a ferrous 5c HS state (*34*, *35*), consistent with their UV−visible absorption spectra (Table 2). We note that the R220H mutant RR spectra did not change with pH and therefore did not undergo iron coordination changes as seen in the Fe^{III} state. For all four mutants, the ν_2 and ν_3 frequencies are slightly downshifted (ca. 2 cm^{-1}) compared to WT *Bj*FixLH, in a manner very similar to that observed for the Fe^{III} met states (Figure 5), again indicating heme flattening and a more expanded heme core size. These observations suggest that the changes in heme planarity, related to removal of the native of Arg 220 residue, are similar to those reported in the X-ray structure of the R220A met Fe^{III} form (*17*) and that they can be extrapolated to the deoxy-Fe^{II} form. Thus, it appears that the removal of Arg220 results in a general flattening of the heme of FixL in both its Fe^{III} and Fe^{II} redox states,

independent of the oxidation state of the heme iron in its high-spin five-coordinated state.

Vinyl Modes. The vinyl $\nu_{C=C}$ stretching mode in the RR spectrum of the WT protein is split, exhibiting two components at 1616 and 1623 cm^{-1} and indicating slightly different environments or geometries for the two vinyl substituents with respect to the heme plane (*38*), while the vinyl $\delta_{C\beta CaCb}$ bending modes are observed as a single band at 409 cm^{-1}. The vibrational frequencies of both modes are not influenced by the mutation, similar to what was observed in the RR spectra of the corresponding Fe^{III} met states (Figure 5). These observations indicate that the heme pocket environment near the vinyl groups remains unchanged upon mutation of Arg220.

Propionate Mode. For the wild-type protein, the propionate $\delta_{C\beta CcCd}$ bending mode band is split, as was seen for the corresponding Fe^{III} met state, with two bands at 365 and 381 cm^{-1}. A similar splitting was also reported for the Fe^{II} deoxy RR spectrum of *Rm*FixL (*16*, *40*) but was not discussed. Both bands are modified upon mutation of Arg220 although not in the same manner. The 365 cm^{-1} band is slightly downshifted to 363 cm^{-1} for all mutants, and its relative intensity appears not to alter (Table 2). In contrast, the 381 cm^{-1} band not only downshifts in frequency upon mutation (by 3 cm^{-1} for R220Q, and 5 cm^{-1} for R220H, R220I, and R220E), but also changes in relative intensity (Table 2). As discussed above, we can assign the propionate RR bands on the basis of the X-ray crystal structures of *Bj*FixLH (*11*). The band at 365 cm^{-1} shows only minor frequency changes upon mutation and is therefore attributed to the propionate 6 group, which is not expected to be in interaction with R220 according to the crystal structure (*12*). The other band at 381 cm^{-1} is attributed to the propionate 7 group which is H-bonded to R220 in the Fe^{II} deoxy state (*12*) and is thus expected to exhibit the most dramatic changes in vibrational frequency upon substitution of the Arg 220 residue which severs this H-bond (Table 2). For all four mutants, the downshifts of the $\delta_{C\beta CcCd}$ bands are correlated with decrease of the ν_9 band frequency from 252 cm^{-1} in the wild-type protein to 249 cm^{-1}, which can be ascribed to a weakening or loss of H-bonding to the propionate groups (*39*). Thus, the observed downshift of the propionate 7 $\delta_{C\beta CcCd}$ frequency (at 381 cm^{-1} for WT, Figure 5) is consistent with a loss of H-bonding to this group upon mutation. The similar frequencies of the $\delta_{C\beta CcCd}$ bending mode for the four mutants indicate that none of the genetically introduced residues donates additional H-bonds to the propionate 7 group. Evidently, only arginine is capable of H-bonding to the propionate groups, which is important to ensure its complete displacement away from the heme Fe oxygen binding site.

The $\delta_{C\beta CcCd}$ mode band intensity is related to the coupling between the Soret transition and the propionate 7 group geometry with the heme plane (*41*); the more the propionate group is in-plane, the more its corresponding RR band will be resonantly enhanced. Compared to that of the wild-type protein, the propionate 7 bending mode intensity is slightly increased in the R220Q mutant and sizeably increased in both the R220H and R220I mutants (Table 2). This indicates that the propionate 7 geometry is modified upon R220 mutation, consistent with the X-ray structure of the met R220A mutant (*17*). For the R220E mutant (Table 2), the considerable attenuation of the propionate 7 $\delta_{C\beta CcCd}$ mode RR band at 376 cm^{-1} band could be due to an unusual, more out-of-plane geometry of the propionate 7 group (*41*) imposed by steric constraints or possibly an electrostatic (repulsive) interaction between the propionate group and the nearby deprotonated, negatively charged Glu side chain (see above).

For the R220H, R220Q, and R220I mutants, the ν_8 band at 341 or 344 cm^{-1} (Figure 6), which is ascribed to a combination of pyrrole stretching and propionate substituent bending modes (*27*, *42*), is seen to lose intensity upon mutation (Table 2) and the γ_6 mode at 332 cm^{-1} (pyrrole tilting mode (*27*)) becomes more intense, indicating an increased flexibility for the propionate groups (*39*, *43*). These intensity changes are greater for the R220H and R220I mutants than for the R220Q mutant. In contrast, the $\nu_8-\gamma_6$ spectral region for the R220E mutant is very similar to that of WT protein (where the propionate 7 group is H-bonded with Arg 220), indicating more rigid propionate groups. In both cases, this rigidity could be attributed to electrostatic interactions between the residue 220 and the propionates, consistent with the negatively charged Glu 220 proposed above.

Thus, for the Fe^{II} deoxy states of WT *Bj*FixL mutants, we observe in general that both (i) the intensity of the RR band due to the propionate 7 heme group and (ii) its flexibility increased following the order: R220E $\approx$ WT $<$ R220Q $<$ R220H $\approx$ R220I (Table 2).

To summarize the RR results of the propionate groups in the Fe^{II} state of FixL: (i) We have been able to assign the 365 and 381 cm^{-1} RR bands in the Fe^{II} deoxy state of WT FixL to the heme propionate 6 and 7 groups, respectively. For the Fe^{III} met state, they were observed at 374 and 385 cm^{-1}, respectively. (ii) Replacement of Arg 220 with other residues does not conserve the H-bond interaction between residue 220 and the heme propionate 7 group, which in turn (iii) results in an increase in propionate flexibility and rotation of the propionate 7 group more in-plane with the heme group (Figure 6 and see refs *11* and *17*). An exception to this observation occurs for the Glu 220 mutation where an unusual out-of-plane propionate geometry is reflected, most likely due to negative electrostatic charge of the Glu side chain.

Fe^{II}−Histidine Mode. The RR band corresponding to the ν_{Fe-His} stretching mode is readily observed in heme (b-type) proteins, where the central iron is in the Fe^{II} 5c HS state, typically around 216−220 cm^{-1} in Mb and Hb (*27*, *34*). Both the vibrational frequency and the relative intensity of this ν_{Fe-His} RR band provide structural information concerning the heme Fe^{II}−His coordination. In *Bj*FixLH, the ν_{Fe-His} stretching mode arising from the proximal His200 was observed at 219 cm^{-1} for the WT (Figure 6). This frequency is somewhat higher than that reported for *Rm*FixL at 209−212 cm^{-1} (*40*), but similar to that previously reported (218 cm^{-1}) for *Bj*FixLH (*35*). For the R220H, R220I, R220Q, and R220E mutants, the ν_{Fe-His} stretching mode is observed at lower frequency, indicating a weakening of the Fe−His_{200} bond (Table 2). This observation is consistent with the lengthening of the Fe−His_{200} bond (+0.31 Å) reported in the X-ray crystal structure of the R220A mutant of met-*Bj*FixLH (*17*). However, the relative intensity of the ν_{Fe-His} stretching mode band of the R220I, R220Q, and R220E mutants is increased as compared to that of WT. The

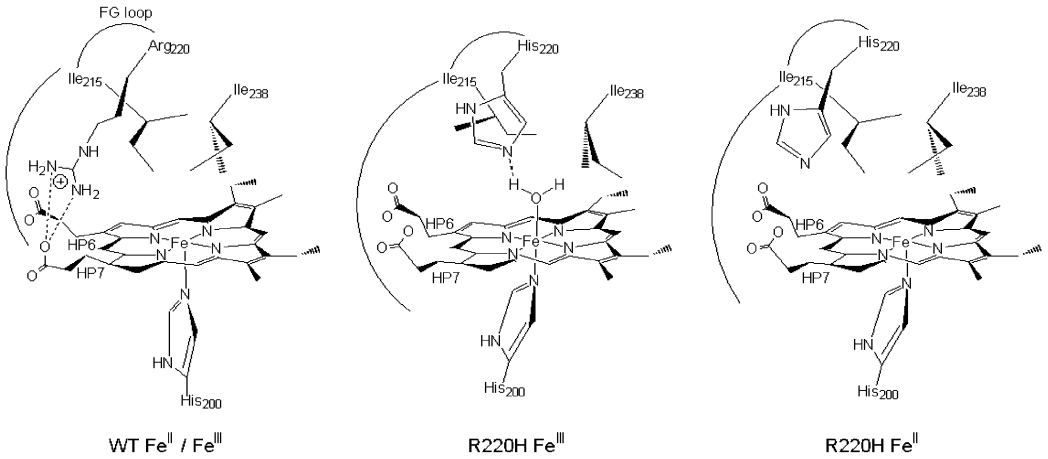

FIGURE 7: Schematic of the structural modifications for the Fe^{III} and Fe^{II} states of the R220H *Bj*FixLH mutant at neutral pH as compared to wild type.

enhancement of the ν_{Fe-His} band intensity can be attributed to the increase of both the azimuthal and tilt angles of the Fe−His unit (*44*), consistent with the crystallographic structure of the R220A met-*Bj*FixLH mutant, which indicates a change of the orientation of the imidazole ring with respect to the heme pyrrole nitrogen atoms and an increase in tilt in the Fe−His bond with respect to the heme plane (*17*). For the R220H mutant, which exhibits the same ν_{Fe-His} frequency as the WT protein, the band intensity is markedly increased, suggesting significant increase in tilt and/or azimuthal angles (*17*, *44*).

DISCUSSION

Arginine 220 is a strictly conserved residue in FixL oxygen sensors that has been shown to be important for selective ligand affinity (*21*) and histidine kinase inactivation (*17*). The specific structural modifications resulting from the mutation of Arg220 we have identified here can be related to functional differences, especially with respect to the k_{on} values for O_2 and CO previously published, thus providing further information on the ligand selectivity mechanism (*21*). In addition, the *Bj*FixLH R220H mutant unexpectedly exhibits pH- and redox-dependent heme iron-coordination changes, which is reminiscent of some WT myoglobins and of *Ec*Dos but is completely unprecedented for FixL proteins. Our findings that the *Bj*FixLH R220H mutant can switch from a six-coordinated high-spin to a five-coordinated high-spin heme iron state upon Fe^{III}/Fe^{II} redox state change reveal the potential of engineering FixL into a redox sensor as well as an oxygen sensor, as well as providing new insights into the mechanism of oxygen sensing in general for these PAS heme-based sensors.

The R220H Mutant. Fe^{III} State. The R220H mutant exhibits a unique behavior not previously observed for FixL proteins. At pH 7.4, the heme iron is six-coordinated HS in the Fe^{III} state, unlike WT and the other mutants, which are all 5c HS. At low pH (e.g., pH 4), the iron R220H mutant is completely in a 5c HS state as determined by UV−visible absorption, RR, and EPR spectroscopies. The pH-dependent 5c ↔ 6c transition of the R220H Fe^{III} iron is probably due to a single protonation of a heme pocket residue with an apparent pK_a value of 5.7 (Figure 2). This value is compatible with that of a distal histidine residue, since in several hemo- or myoglobins, pK_a of the distal His(E7) residue is observed in the pH range 4.3 for *SW*Mb (*45*) to 6.3 for midge larva Hb (*46*). Thus, the sixth ligand of the His mutant might be considered to be the actual His220 side chain itself. However, such resulting Fe^{III}−bis-histidine coordination usually results in low-spin Fe^{III} states (Table 1 and ref *47*), unlike the high-spin state we observe here. Thus, we propose that the sixth ligand in the R220H *Bj*FixLH Fe^{III} state is most likely a water molecule since the spectroscopic features are very similar to that of *SW* met myoglobin. The proposed structure of the heme pocket at pH 7.4 is schematically shown in Figure 7, where the Fe^{III} center is coordinated with a water molecule that is itself H-bonded with the His residue at position 220. At low pH, this His220 becomes protonated, thus destabilizing the coordination of the water molecule with the Fe^{III} center. This resulting structure is similar to that of *SW*Mb (*15*) and *Ec*Dos (*9*), but in *Ec*Dos the Fe^{III} is low-spin (*7*). The presence of a water molecule and His220 pointing inside the heme pocket of *Bj*FixLH suggests a more hydrophilic heme pocket whose structure, especially with respect to the hydrophobic Ile238 and Ile215 side chain positions (Figure 7), should be similar to that reported in the FixL crystallographic structures of all six coordinated states (*12*). On the basis of the similarity of the RR spectra in the propionate bending mode region for the R220H mutant in the Fe^{III} deoxy and $Fe^{II}-O_2$ states (*21*), we further expect displacement of the crucial FG loop (including Ile215), as observed for the R220H $Fe^{II}-O_2$ state where His220 interacts via a hydrogen bond with the O_2 ligand (*21*). Displacement of Ile215 is further supported by the results obtained for the I210H mutant of *Rm*FixL, which exhibits both an isoleucine (Ile209 = Ile215 in *Bj*FixL) and a histidine residue around the heme iron and still has a hydrophobic heme pocket with no coordinated water molecule in the met state (*16*). By analogy, Ile215 and the water molecule should not be present together in the heme vicinity of the *Bj*FixLH R220H mutant.

In contrast, for the low pH RR spectrum of the *Bj*FixLH R220H mutant (Figure 5) the $\nu_{C=C}$ vinyl stretching frequency is identical to that of WT at pH 7.4, where it is known that Arg220 is pointing away from the heme iron while Ile238 is pointing toward the iron. The heme vinyl groups of *Bj*FixL are in van der Waals contact with Ile238 (and Leu236) (*14*), therefore the lack of change in the vinyl frequencies indicating that Ile238 of the hydrophobic triad is still pointing toward the iron for the R220H mutant. This implies that the

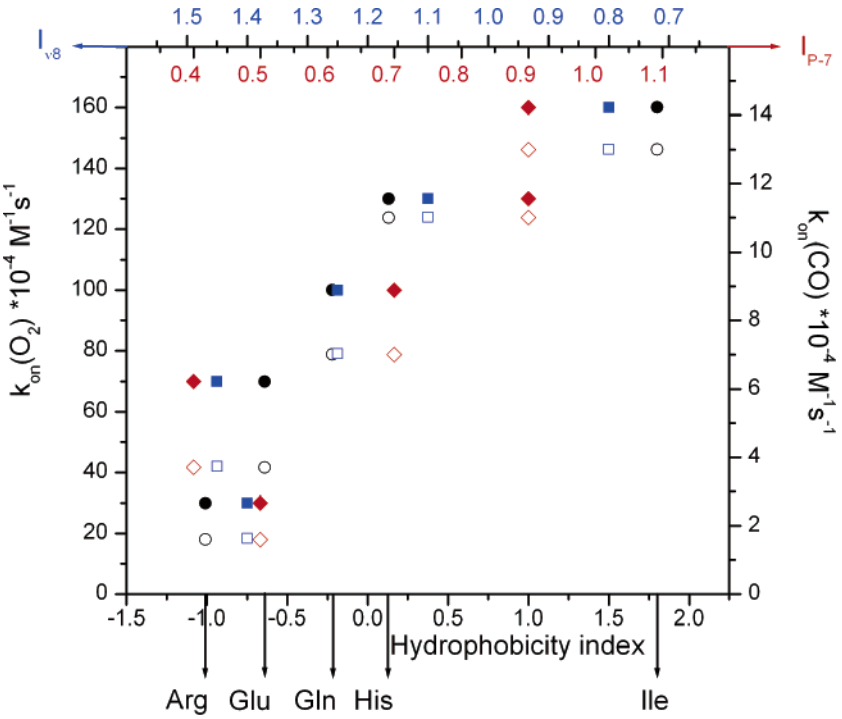

FIGURE 8: Correlation between the k_{on} values for O_2 (filled symbols) and CO (empty symbols) (*24*) and the hydrophobicity index of the residue in position 220 (●○) (*60*), the ν_8 Raman band relative intensity $I_{\nu 8}$ (■□), and the propionate 7 $\delta_{C\beta CcCd}$ band relative intensity I_{P-7} (◆◇), both reported in Table 2.

protonated His220 residue is pointing toward the outside of the heme pocket and thus results in a small highly hydrophobic heme pocket in the immediate vicinity of the central heme iron, similar to that of the wild-type Fe^{III} protein (*10*). Still, we do not detect a significant H-bond interaction between His220 and the propionate 7 group as is present in the WT. This lack of H-bond can be due to the reduced length of the His side chain as compared to arginine or to protonation of propionate 7 at pH 4.4, since heme propionate usually ionizes with a pK_a of 5−6 (*48*).

Fe^{II} State. Upon reduction of the R220H mutant from the met Fe^{III} to the Fe^{II} deoxy state, the coordinated water molecule is lost, resulting in a 5c HS Fe^{II} heme iron state. A similar behavior is observed for most myo- and hemoglobins; however, in these cases, the water molecule is maintained in the distal pocket and still interacts via a H-bond with the His(E7) residue (*15*). For myo- and hemoglobin, this results in steric hindrance in the distal pocket and low k_{on} values for both O_2 and CO binding (*49*). For the R220H mutant, the k_{on} values for O_2 and CO bonding are similar to those reported for the R220I and R220Q mutants (*21*). This means that no additional steric hindrance is noticed in the distal pocket of the R220H mutant and strongly suggests that the water molecule ligated to Fe^{III} in the met form is not situated near the Fe−O_2/CO binding site in the deoxy Fe^{II} state. Moreover, analysis of the vinyl substituent frequencies indicates that the vinyl environment is similar in the wild-type protein and in the R220H mutant. This indicates that the Ile238 side chain is not directed toward the vinyls as in the R220H Fe^{III} state, but pointing toward the iron as in the wild-type protein (Figure 7).

Analysis of the RR spectra of the Fe^{II} deoxy state indicates highly flexible propionates in a similar way as for the R220I mutant. However, the structure of the Fe^{II} R220H mutant is not exactly that of the other mutants, as indicated by increase of both frequency and intensity of the ν_{Fe-His} stretching mode, indicating a stronger Fe−His interaction.

Redox Behavior of the R220H Mutant. In the Fe^{III} state, the R220H *Bj*FixLH mutant exhibits a similar high-spin six-coordinated structure as that of myoglobin, with both a His and a water molecule in the axial positions (*15*). Upon reductive titration, the water ligand is displaced and the iron becomes five-coordinated (His−Fe). Therefore, for both proteins, the observed redox midpoint potential corresponds to the redox couple His−Fe^{III}−OH_2/His−Fe^{II}. However, for *SW*Mb the water ligand remains in the heme pocket, whereas for the R220H *Bj*FixLH mutant, the water molecule exits the heme pocket, with substantial FG loop shift. The absence of hysteresis in both cases indicates that rapid interconversion is observed between both redox state stuctures, implying a relatively low activation energy for the hydrophobic to hydrophilic transition in the R220H *Bj*FixLH mutant despite the fact that it is associated with a shift of the FG loop. This observation is generally consistent with the high flexibility expected for PAS domains (*3*). The electrochemical behavior of the R220H *Bj*FixLH mutant protein is quite similar to that reported for the oxygen/redox sensor *Ec*Dos. Upon reductive titration, the water ligand of the low-spin *Ec*Dos His−Fe^{III}−OH_2 complex is replaced by a methionine residue leading to a 6c His−Fe^{II}−Met complex (*9*). Again in this case, no hysteresis is reported for the redox titration (*8*). This implies that the structural modifications related to the ligand exchange are rapid and reversible on the time scale of the electrochemical experiment and the 67 mV redox potential reported for *Ec*Dos corresponds to the redox couple His−Fe^{III}−OH_2/His−Fe^{II}−Met. The recent crystallographic structures reported for the Fe^{III} state of *Ec*Dos indicate that the water ligand is not stabilized by a histidine residue, consistent with a pH-independent coordination state, and comparison of the *Ec*Dos crystallographic structures of both redox states

indicates substantial stiffening of the FG loop upon reduction (*50*).

The Fe^{II} Deoxy States: Functional Implications. The Fe^{II} deoxy state is a key state in FixL functioning. Mutation of Arg 220 to Ile, His, Gln, or Glu does not alter *Bj*FixLH iron coordination (5c) and spin state (HS) in the Fe^{II} deoxy state, as revealed by UV−visible, EPR, and resonance Raman spectra (see above for the R220H mutant). Still, several structural changes in the heme vicinity are reported. First, the RR spectra of these mutants clearly indicate that removal of the Arg 220 side chain results in the net loss of an H-bond interaction on the heme propionate 7 group consistent with the crystal structure (*17*), where Arg220 is engaged in a H-bond interaction with the heme propionate 7 group. Comparing the properties of the arginine side chain with those others in the series of mutants studied here that are capable of donating H-bonds (e.g., glutamine, histidine), we found that it is probably a combination of the length of the Arg side chain and its positive charge that is largely responsible for H-bonding with the propionate 7 group. For the R220E mutant, as deduced from the electrochemical redox titrations (see Results), the Glu side chain is most likely deprotonated and thus incapable of donating a H-bond. Disruption of this H-bond also affects the H-bond network near the propionate 6 group (Table 2). This leads to modifications of the propionates' flexibility and of the propionate 7 geometry as gauged by several propionate sensitive modes (e.g., $\delta_{C\beta CcCd}$, γ_6 modes) in the low-frequency RR spectra.

Protein Conformational Changes. Key structural elements of signal initiation in oxygen-sensing in FixL have been proposed to be the change in heme planarity and concomitant changes in H-bond interactions with respect to the heme propionate groups when O_2 dissociates from the Fe^{II} atom (*12*). Here, we have a unique opportunity to investigate the structural changes occurring when the hydrogen bond between residue 220 and propionate 7 is broken without the presence of O_2. The RR spectra of the Fe^{II} redox states of the four R220I, R220H, R220Q, and R220E *Bj*FixLH mutants indicate an increase in the heme planarity as compared to WT. In addition, the ν_{Fe-His} stretching mode in the Fe^{II} deoxy state spectra shows that frequency decreases indicate a weakening or lengthening of the $Fe-His_{200}$ bond, as well as increases in band intensity which can be ascribed to changes in the orientation of the imidazole plane toward the porphyrin ring, with increase of the tilt and/or the azimuthal angle (*44*). The above-mentioned structural changes are similar to those reported upon O_2 fixation in the wild-type protein (*10*−*12*). Thus, part of the heme structural changes usually attributed to O_2 fixation appears to be induced solely by the disruption of the H-bond between propionate 7 and Arg220. This H-bond places the arginine, which is part of the critical FG loop, in a position pointing away from the O_2 binding site, thus "locking" the protein in a particular conformational state. The rupture of this H-bond as seen in all the mutants studied here induces a "release" of the locked protein conformation, which results in geometrical rearrangement of both the propionate 6 and 7 groups along with concomitant changes in heme planarity as well as heme $Fe^{II}-His_{200}$ bond length and histidine orientation. Since the His_{200} is part of the α-helix connected to the critical FG loop (*10*), whose movement is thought to be important in signal transduction and ligand discrimination, the observed changes in its orientation with the heme when the Arg220-propionate 7 H-bond interaction is removed should be transmitted to the α-helix and thus to the FG loop.

In the R220H and R220I mutants, residue 220 is pointing outside the heme pocket in the Fe^{II} deoxy states (see above for the R220H mutant). This indicates that the interaction between residue 220 and propionate 7 is not required to maintain residue 220 outside of the heme pocket, but that this structure is thermodynamically favored when no ligand is bound to the iron. The results presented here, together with those previously reported (*21*), provide further evidence that the H-bond between Arg220 and the propionate 7 group of the heme is important for ligand discrimination in the O_2 sensor FixL. X-ray crystallographic (*12*) and RR data (*21*) show that the native Arg220 residue does not interact with CO in the $Fe^{II}-CO$ state but remains H-bonded with the propionate 7 group like in the Fe^{II} deoxy state as seen by the crystal structure (*12*) and in the RR work reported here. Only when O_2 is bound does the Arg220 residue rupture its H-bond with the propionate 7 heme group and move toward the O_2 ligand to interact with it. The results obtained for the histidine mutant indicate that, upon all ligand binding (H_2O, CO, and O_2) (*21*), structural reorganization of the heme pocket occurs, implying displacement of the G β-sheet and FG loop residues (Leu236, Ile238, and residue 220), and no ligand discrimination is observed. This indicates that the 6c thermodynamically stable structure of the mutant is the one having residue 220 pointing inside the heme pocket. Extrapolation of this observation to the WT protein strongly suggests that the role of the strong interaction between propionate 7 and Arg220 is to prevent displacement of this residue inside the heme pocket upon binding of ligands other than O_2.

O_2 and CO k_{on} Binding Rates. In our previous article (*21*), we were able to relate the observed O_2 k_{off} values for the mutants with the formation of H-bonds with the bound O_2 molecule; however, the variation in k_{on} values could not be explained. The structural modifications reported here for the Fe^{II} deoxy states of the mutants may be related to the reported k_{on} values for the binding of the O_2 and CO ligands. We previously showed that mutation of Arg220 in the *Bj*FixL hemodomain leads to an increase in the k_{on} values for both diatomic ligands (*21*). Our RR results indicate that the conformations of the vinyl substituents remain unchanged for the mutants in their Fe^{II} deoxy states. Since the vinyl substituents are in van der Waals contact with the Leu236/Ile238 residues of the hydrophobic triad (*14*), this observation indicates that the positions of the Leu236 and Ile238 residues (*10*) in the heme distal pocket, and thus its degree of hydrophobicity, remain largely unchanged in the vicinity of the $Fe-O_2$/CO binding site. Thus, hydrophilic residues such as His or Gln at position 220 should point away from the $Fe-O_2$ binding site of the heme pocket, as Arg220 does in the WT protein, leading to a more or less unchanged FG loop position as compared to the WT Fe^{II} deoxy protein. Therefore, differences in the observed k_{on} values for the mutants cannot be explained by steric changes around the iron atom. Two other explanations may be proposed. One is that the interaction between Arg220 and propionate 7 is localized in the entrance channel of the ligands, resulting in steric hindrance for ligand approach and binding. This

proposal is further supported by the crystallographic structure where Arg220 interacts with solvent water molecules (*10*). The second explanation is that increase in the His200 tilt and/or azimuthal angles (see above) results in a decrease of the repulsion energy between the imidazole carbon atoms of His200 and the porphyrin nitrogen atom, leading to a decrease in the activation energy of bond formation between the iron and the ligand (*51*).

We rather observe a correlation between both the k_{on} values for O_2 and CO and the geometry/flexibility of the propionates indicated by the ν_8 and $\delta_{C\beta CcCd}$(P-7) relative intensities (Figure 8) than with the ν_{Fe-His} frequency. Moreover, we also notice that the k_{on} values for CO and O_2 binding correlate with the hydrophobicity index of the residue in position 220 (*52*), which has to be an important parameter since Arg220 is interacting with a solvent molecule in the wild-type *Bj*FixLH protein (*10*) indicative of a fairly accessible Arg220−propionate 7 cluster. Figure 8 shows that high k_{on} values for both ligand bindings correlate with a high HI for residue 220, with low ν_8 intensity indicative of flexible propionates and with high $\delta_{C\beta CcCd}$(P-7) intensity indicative of more in-plane propionate 7 geometry.

In the wild-type *Bj*FixLH protein, the interaction of propionate 7 with Arg220 is based on an electrostatic attraction together with H-bond formation that rigidifies propionate 7 in a fixed geometry ($I_{\nu 8}$ high and I_{P-7} low). This results in the formation of a rigid hydrophilic cluster, probably also involving water molecules according to the X-ray structure (*10*). For the R220E mutant, the propionate 7 group appears to be more rigid as seen by RR, which we attribute to electrostatic repulsion between the propionate 7 and the negatively charged glutamate. Because this negatively charged residue is hydrophilic, this interaction probably induces formation of a cluster also containing water molecules. As in the wild-type protein, this interaction rigidifies propionate 7 in a fixed geometry. In both cases, the k_{on} values for O_2 and CO binding are low. For the R220H and R220I mutants, RR analysis of the deoxy state indicates highly flexible propionates ($I_{\nu 8}$ low and I_{P-7} high), rotated away from the heme plane, and we observe an increase in the k_{on} values. For the R220Q mutant, we observe a slight increase in the propionate flexibility together with slight rotation away from the heme plane, and we report an increase in the k_{on} values. The structural differences observed between the R220I and R220Q mutants may be due to weak interaction of the Gln with propionate 7 probably via water molecule, since glutamine (HI = −0.22) is much more hydrophilic than isoleucine (HI = +1.8) (*52*). This proposal is consistent with the slight increase of the $\delta_{C\beta CcCd}$ frequency reported for the R220Q mutant (Table 2).

We finally propose that both the heme propionate 7 and Arg220 are located in the entrance channel of the ligands and that formation of a hydrophilic cluster involving both groups and probably water molecules hinders the approach of both O_2 and CO molecules, most likely by steric hindrance. Hydrophobicity of the propionates has been previously shown to influence the k_{on} rates for both O_2 and CO binding in myoglobin (*53*). For *Bj*FixL, this proposal is further supported by molecular dynamics simulations of ligand dynamics in the heme environment of wild-type and mutant FixLH (Lambry, J.-C., Liebl, U., and Vos, M. H., unpublished results). Thus, the size of the 220 residue also has to be an essential parameter for the ligand entrance rate.

CONCLUSION

In both the met Fe^{III} and Fe^{II} deoxy forms of the wild-type *Bj*FixLH protein, the heme pocket is characterized by a high degree of hydrophobicity, which is mainly due to the presence of the hydrophobic triad Ile215/Leu236/Ile238 conserved in several sensor proteins presenting PAS domains. In both redox states, this peculiar heme pocket structure is associated with a fully active histidine kinase domain. In the deoxy state, the lack of perturbation on the heme vinyl groups strongly suggests that the structure of the heme pocket and the position of the FG loop remain unchanged upon mutation of Arg220. Thus, we expect these mutations to not strongly affect the kinase activity of the full length Fe^{II} enzyme. In contrast, we report structural modifications at the level of the heme propionate groups for the Fe^{II} and Fe^{III} resting states upon R220 mutation that are related to the k_{on} values for ligand binding previously published (*21*). The interaction between propionate 7 and Arg220 is essential to lock the protein structure and enhance ligand discrimination, by maintaining Arg220 outside of the heme pocket upon CO and NO binding. However, this interaction appears also to be responsible for the low k_{on} values reported for ligand binding, most likely by generating steric hindrance in the ligand entrance channel.

We also report a unique six-coordinated FixL Fe^{III} state of the R220H mutant exhibiting a heme pocket, where the His220 is pointing toward the inside of the heme pocket and interacting with a bound H_2O ligand. We report for the first time for FixL that hydrophobicity of the heme pocket, and the position of the FG loop, can be modified by only changing the redox state of the metal. This should result in a partial inhibition of the histidine kinase activity. Thus, by changing Arg220 into His220, the function of the *Bj*FixLH protein is strongly altered, and the protein becomes redox-sensitive. We notice that this effect appears to be very specific to histidine and that substitution of Arg220 by another hydrophilic residue capable of H-bonding (e.g., glutamine) does not allow the structural switch by changing the redox state of the protein.

SUPPORTING INFORMATION AVAILABLE

Oxidative and reductive redox titrations for the R220H variant of *Bj*FixLH at pH 7.6. This material is available free of charge via the Internet at http://pubs.acs.org.

REFERENCES

1. Gilles-Gonzalez, M.-A., and Gonzalez, G. (2005) Heme-based sensors: defining characteristics, recent developments, and regulatory hypotheses. *J. Inorg. Biochem. 99*, 1−22.
2. Jain, R., and Chan, M. K. (2003) Mechanisms of ligand discrimination by heme proteins. *J. Biol. Inorg. Chem. 8*, 1−11.
3. Vreede, J., van der Horst, M. A., Hellingwerf, K. J., Crielaard, W., and van Aalten, D. M. F. (2003) PAS Domains. *J. Biol. Chem. 278*, 18434−18439.
4. Gilles-Gonzalez, M.-A., Ditta, G. S., and Helinski, D. R. (1991) A haemoprotein with kinase activity encoded by the oxygen sensor of *Rhizobium meliloti*. *Nature 350*, 170−172.
5. Dioum, E. M., Rutter, J., Tuckerman, J. R., Gonzalez, G., Gilles-Gonzalez, M.-A., and McKnight, S. L. (2002) NPAS2: a gas-responsive transcription factor. *Science 298*, 2385−2387.

6. Chang, A. L., Tuckerman, J. R., Gonzalez, G., Mayer, R., Weinhouse, H., Volman, G., Amikam, D., Benziman, M., and Gilles-Gonzalez, M.-A. (2001) Phosphodiesterase A1, a regulator of cellulose synthesis in *Acetobacter xylinum*, is a heme-based sensor. *Biochemistry 40*, 3420−3426.
7. Delgado-Nixon, V. M., Gonzalez, G., and Gilles-Gonzalez, M.-A. (2000) Dos, a heme-binding PAS protein from *Escherichia coli*, is a direct oxygen sensor. *Biochemistry 39*, 2685−2691.
8. Sasakura, Y., Hirata, S., Sugiyama, S., Suzuki, S., Taguchi, S., Watanabe, M., Matsui, T., Sagami, I., and Shimizu, T. (2002) Characterization of a direct oxygen sensor heme protein from *Escherichia coli*. Effects of the heme redox states and mutations at the heme-binding site on catalysis and structure. *J. Biol. Chem. 277*, 23821−23827.
9. Kurokawa, H., Lee, D.-S., Watanabe, M., Sagami, I., Mikami, B., Raman, C. S., and Shimizu, T. (2004) A redox-controlled molecular switch revealed by the crystal structure of a bacterial heme PAS sensor. *J. Biol. Chem. 279*, 20186−20193.
10. Gong, W., Hao, B., Mansy, S. S., Gonzalez, G., Gilles-Gonzalez, M.-A., and Chan, M. K. (1998) Structure of a biological oxygen sensor: a new mechanism for heme-driven signal transduction. *Proc. Natl. Acad. Sci. U.S.A. 95*, 15177−15182.
11. Gong, W., Hao, B., and Chan, M. K. (2000) New mechanistic insights from structural studies of the oxygen-sensing domain of *Bradyrhizobium japonicum* FixL. *Biochemistry 39*, 3955−3962.
12. Hao, B., Isaza, C., Arndt, J., Soltis, M., and Chan, M. K. (2002) Structure-based mechanism of O_2 sensing and ligand discrimination by the FixL heme domain of *Bradyrhizobium japonicum*. *Biochemistry 41*, 12952−12958.
13. Miyatake, H., Mukai, M., Park, S.-Y., Adachi, S., Tamura, K., Nakamura, H., Nakamura, K., Tsuchiya, T., Iizuka, T., and Shiro, Y. (2000) Sensory mechanism of oxygen sensor FixL from *Rhizobium meliloti*: crystallographic, mutagenesis and resonance Raman spectroscopic studies. *J. Mol. Chem. 301*, 415−431.
14. Key, J., and Moffat, K. (2005) Crystal structure of deoxy and CO-bound *bj*FixLH reveal details of ligand recognition and signaling. *Biochemistry 44*, 4627−4635.
15. Quillin, M. L., Arduini, R. M., Olson, J. S., and Phillips, G. N., Jr. (1993) High-resolution crystal structures of distal histidine mutants of sperm whale myoglobin. *J. Mol. Biol. 234*, 140−155.
16. Mukai, M., Nakamura, K., Nakamura, H., Iizuka, T., and Shiro, Y. (2000) Roles of Ile209 and Ile210 on the heme pocket structure and regulation of histidine kinase activity of oxygen sensor FixL from *Rhizobium meliloti*. *Biochemistry 39*, 13810−13816.
17. Dunham, C. M., Dioum, E. M., Tuckerman, J. R., Gonzalez, G., Scott, W. G., and Gilles-Gonzalez, M.-A. (2003) A distal arginine in oxygen-sensing heme-PAS domains is essential to ligand binding, signal transduction, and structure. *Biochemistry 42*, 7701−7708.
18. Tuckerman, J. R., Gonzalez, G., Dioum, E. M., and Gilles-Gonzalez, M.-A. (2002) Ligand and oxidation-state specific regulation of the heme-based oxygen sensor FixL from *Sinorhizobium meliloti*. *Biochemistry 41*, 6170−6177.
19. Perutz, M. F., Paoli, M., and Lesk, A. M. (1999) FixL, a haemoglobin that acts as an oxygen sensor: signalling mechanism and structural basis of its homology with PAS domains. *Chem. Biol. 6*, R291−R297.
20. Liebl, U., Bouzhir-Sima, L., Négrerie, M., Martin, J.-L., and Vos, M. H. (2002) Ultrafast ligand rebinding in the heme domain of the oxygen sensors FixL and Dos: general regulatory implications for heme-based sensors. *Proc. Natl. Acad. Sci. U.S.A. 99*, 12771−12776.
21. Balland, V., Bouzhir-Sima, L., Kiger, L., Marden, M. C., Vos, M. H., Liebl, U., and Mattioli, T. A. (2005) Role of arginine 220 in the oxygen sensor FixL from *Bradyrhizobium japonicum*. *J. Biol. Chem. 280*, 15279−15288.
22. Rodgers, K. R., and Lukat-Rodgers, G. S. (2005) Insights into heme-based O_2 sensing from structure−function relationships in the FixL proteins. *J. Inorg. Biochem. 99*, 963−977.
23. Boussac, A., Un, S., Horner, O., and Rutherford, A. W. (1998) High-spin states ($S \geq {}^5/_2$) of the photosystem II manganese complex. *Biochemistry 37*, 4001−4007.
24. Ferguson, W. J., Braunschweiger, K. I., Braunschweiger, W. R., Smith, J. R., McCormick, J. J., Wasmann, C. C., Jarvis, N. P., Bell, D. H., and Good, N. E. (1980) Hydrogen ion buffers for biological research. *Anal. Biochem. 104*, 300−310.
25. Lexa, D., Saveant, J.-M., and Zickler, J. (1977) Electrochemistry of vitamin B12. 2. Redox and acid−base equilibria in the B12a/B12r system. *J. Am. Chem. Soc. 99*, 2786−2790.
26. Wilson, G. S. (1978) Determination of Oxidation-Reduction Potentials. *Methods Enzymol. 54*, 396−435.
27. Hu, S., Smith, K. M., and Spiro, T. G. (1996) Assignment of protoheme resonance Raman spectrum by heme labeling in myoglobin. *J. Am. Chem. Soc. 118*, 12638−12646.
28. Gilles-Gonzalez, M.-A., Gonzalez, G., and Perutz, M. F. (1995) Kinase activity of oxygen sensor FixL depends on the spin state of its heme iron. *Biochemistry 34*, 232−236.
29. Ikeda-Saito, M., Hori, H., Andersson, L. A., Prince, R. C., Pickering, I. J., George, G. N., Sanders, C. R., II, Lutz, R. S., McKelvey, E. J., and Mattera, R. (1992) Coordination structure of the ferric heme iron in engineered distal histidine myoglobin mutants. *J. Biol. Chem. 267*, 22843−22852.
30. Lukat-Rodgers, G. S., Rexine, J. L., and Rodgers, K. R. (1998) Heme speciation in alkaline ferric FixL and possible tyrosine involvement in the signal transduction pathway for regulation of nitrogen fixation. *Biochemistry 97*, 13543−13552.
31. Palmer, G. (1985). The electron paramagnetic resonance of metalloproteins. *Biochem. Soc. Trans. 13*, 548−560.
32. Shifman, J. M., Gibney, B. R., Sharp, R. E., and Dutton, P. L. (2000) Heme redox potential control in de novo designed four-α-helix bundle proteins. *Biochemistry 39*, 14813−14821.
33. Van Dyke, B. R., Saltman, P., and Armstrong, F. A. (1996) Control of myoglobulin electron-transfer rates by the distal (nonbound) histidine residue. *J. Am. Chem. Soc. 118*, 3490−3492.
34. Spiro, T. G., and Li, X.-Y. (1988) in *Biological applications of Raman spectroscopy* (Spiron, T. G., Ed.) Vol. 3, pp 1−37, Wiley-Interscience, New York.
35. Tomita, T., Gonzalez, G., Chang, A. L., Ikeda-Saito, M., and Gilles-Gonzalez, M.-A. (2002) A comparative resonance Raman analysis of heme-binding PAS domains: heme iron coordination structures of the *Bj*FixL, *Ax*PDEA1, *Ec*Dos, and *Mt*Dos proteins. *Biochemistry 41*, 4819−4826.
36. Smulevich, G., Mantini, A. R., Paoli, M., Coletta, M., and Geraci, G. (1995) Resonance Raman studies of the heme active site of the homodimeric myoglobin from *Nassa mutabilis*: a peculiar case. *Biochemistry 34*, 7507−7516.
37. Jin, Y., Nagai, M., Nagai, Y., Nagamoto, S., and Kitagawa, T. (2004) Heme structures of five variants of hemoglobin M probed by resonance Raman spectroscopy. *Biochemistry 43*, 8517−8527.
38. Marzocchi, M. P., and Smulevich, G. (2003) Relationship between heme vinyl conformation and the protein matrix in peroxidases. *J. Raman Spectrosc. 34*, 725−736.
39. Gottfried, D. S., Peterson, E. S., Sheikh, A. G., Wang, J., Yang, M., and Friedman, J. M. (1996) Evidence for damped hemoglobin dynamics in a room temperature trehalose glass. *J. Phys. Chem. 100*, 12034−12042.
40. Tamura, K., Nakamura, H., Tanaka, Y., Oue, S., Tsukamoto, K., Nomura, M., Tsuchiya, T., Adachi, S., Takahashi, S., Iizuka, T., and Shiro, Y. (1996) Nature of endogenous ligand binding to heme iron in oxygen sensor FixL. *J. Am. Chem. Soc. 118*, 9434−9435.
41. Cerda-Colon, J. F., Silfa, E., and Lopez-Garriga, J. (1998) Unusual rocking freedom of the heme in the hydrogen sulfide binding hemoglobin from *Lucina pectinata*. *J. Am. Chem. Soc. 120*, 9312−9317.
42. Morikis, D., Champion, P. M., Springer, B. A., Egeberg, K. D., and Sligar, S. G. (1990) Resonance Raman studies of iron spin and axial coordination in distal pocket mutants of ferric myoglobin. *J. Biol. Chem. 265*, 12143−12145.
43. Peterson, E. S., Friedman, J. M., Chien, E. Y. T., and Sligar, S. G. (1998) Functional implications of the proximal hydrogen bonding network in myoglobin: a resonance raman and kinetic study of Leu89, Ser92, His97, and F-swap mutants. *Biochemistry 37*, 12301−12319.
44. Mizutani, Y., and Kitagawa, T. (2001) Ultrafast dynamics of myoglobin probed by time-resolved resonance Raman spectroscopy. *Chem. Rec. 1*, 258−275.
45. Ramdsen, J., and Spiro, T. G. (1989) Resonance Raman evidence that distal histidine protonation removes the steric hindrance to upright binding of carbon monoxide by myoglobin. *Biochemistry 28*, 3125−3128.
46. Akiyama, K., Fukuda, M., Kobayashi, N., Matsuoka, A., and Shikama, K. (1994) The pH-dependent swinging-out of the distal histidine residue in ferric hemoglobin of a midge larve (*Tokunagayusurika akamusi*). *Biochim. Biophys. Acta 1208*, 306−309.
47. Walker, F. A. (2004) Models of the bis-histidine-ligated electron-transferring cytochromes. Comparative geometric and electronic structure of low-spin ferro- and ferrihemes. *Chem. Rev. 104*, 589−561.

48. a. Das, D. K., and Medhi, O. K. (1998) The role of heme propionate in controlling the redox potential of heme: square wave voltammetry of protoporphyrinato IX iron(III) in aqueous surfactant micelles. *J. Inorg. Biochem. 70*, 83−90. b. Matsuoka A., and Shikama, K. (1992) Stability properties of *Aplysia* oxymyoglobin: effect of esterification of the heme propionates. *Biochim. Biophys. Acta 1118*, 123−129.
49. Springer, B. A., Sligar, S. G., Olson, J. S., and Phillips, G. N., Jr. (1994) Mechanisms of ligand recognition in myoglobin. *Chem. Rev. 94*, 699−714.
50. Sato, A., Sasakura, Y., Sugiyama, S., Sagami, I., Shimizu, T., Mizutani, Y., and Kitagawa, T. (2002) Stationary and time-resolved resonance Raman spectra of His^{77} and Met^{95} mutants of the isolated heme domain of a direct oxygen sensor from *Escherichia coli*. *J. Biol. Chem. 277*, 32650−32658.
51. Harutyunyan, E. H., Safonova, T. N., Kuranova, I. P., Popov, A. N., Teplyakov, A. V., Obmolova, G. V., Rusakov, A. A., Vainshtein, B. K., Dodson, G. G., Wilson, J. C., and Perutz, M. F. (1995) The structure of deoxy- and oxy-leghaemglobin from lupin. *J. Mol. Biol. 251*, 104−115.
52. Fauchere, J. L., and Pliska, V. (1983) Hydrophobic parameters of amino acid side chains from the partitioning of *N*-acetyl-amino acid amides. *Eur. J. Med. Chem. 18*, 369−375.
53. Sato, H., Watanabe, M., Hisaeda, Y., and Hayashi, T. (2005) Unusual ligand discrimination by a myoglobin reconstituted with a hydrophobic domain-linked heme. *J. Am. Chem. Soc. 127*, 56−57.

BI051696H